The optimization of mold taper for the Ilva-Dalmine round bloom caster*

M.R. Ridolfi (CSM, Roma),
B.G. Thomas, G. Li (Univ. of Illinois, USA),
U. Della Foglia (Ilva-Dalmine)

To optimize the mold taper, a thermo-mechanical analysis of the cooling and shrinkage taking place inside the solidifying steel shell has been performed together with a heat flow analysis of the liquid slag moving down the interfacial gap between the mold wall and the shell.

Experimental thermocouple measurements in an operating mold were employed to calibrate the model predictions.

Results indicate that taper should decrease greatly from the top to the bottom of the mold, so a multifold taper is recommended.

■ INTRODUCTION

The early stages of solidification in the mold play a fundamental role in the continuous casting process. Several problems originate in the mold, including break-outs and surface defects which can significantly reduce both productivity and quality. Mold taper is one of the few critical, controlable process variables which has an important influence on these phenomena. It is particularly important for the casting of round blooms and billets, which do not have any corners where local shrinkage of the shell can offset inadequate taper.

In order to determine in a non-empirical way the ideal mold taper for a round bloom caster, a numerical modeling study has been performed. The model is based upon the simultaneous solution of the equations which govern the physical phenomena occurring in the mold, which are illustrated schematically in *figure 1*. Thermal phenomena include the convection of superheat through the liquid pool, conduction through the solidifying steel shell, conduction and radiation across the interfacial gap and conduction within the mold. Mechanical phenomena include shrinkage of the steel shell, distortion of the mold, mass and momentum balance on the mold flux layers, which govern their thicknesses.

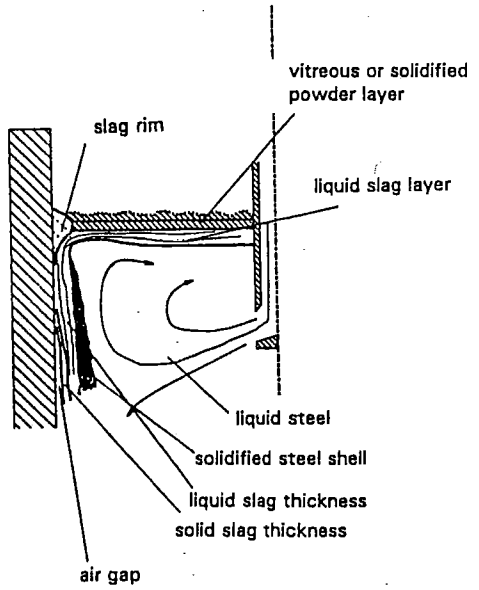

Fig. 1 – Physical phenomena occuring in the mold.

Fig. 1 – Phénomènes physiques se produisant dans la lingotière.

* *Subject of lecture at the ATS Steelmaking Conference 1993 (Paris, 15-16 December, 1993, Session 7).*

Optimisation de la conicité de la lingotière pour la machine de coulée continue de ronds à l'Ilva-Dalmine

M.R. Ridolfi (CSM, Rome),
B.G. Thomas, G. Li (Univ. of Illinois, USA),
U. Della Foglia (Ilva-Dalmine)

Les premiers instants de la solidification en lingotière jouent un rôle fondamental en coulée continue. De nombreux problèmes ont pour origine la lingotière, y compris les percées et les défauts de surface qui peuvent détériorer fortement la productivité et la qualité. La conicité de la lingotière est l'un de ces quelques paramètres critiques du processus qu'il est possible de contrôler et qui a une influence importante sur ces phénomènes. Il est particulièrement important dans le cas de la coulée de blooms ronds et de billettes rondes, pour lesquels il n'existe pas d'angles où une contraction locale de la peau peut compenser une conicité inadaptée.

Pour déterminer de façon non empirique la conicité de lingotière idéale pour une machine à blooms ronds, nous avons effectué une étude de modélisation numérique. Le modèle est fondé sur la résolution simultanée des équations qui gouvernent les phénomènes physiques se produisant dans la lingotière et qui sont illustrés schématiquement sur la figure 1. Les phénomènes thermiques comprennent la convection de la surchauffe à travers le puits liquide, la conduction à travers la peau en cours de solidification, la conduction et le rayonnement dans l'espace interfacial et la conduction à l'intérieur de la lingotière. Les phénomènes mécaniques comprennent la contraction de la peau, la déformation de la lingotière, les équilibres entre les masses et entre les moments des forces s'exerçant au niveau des couches de poudres de lingotière et qui gouvernent leur épaisseur.

Ces phénomènes sont intimement liés car la quantité de chaleur transférée de la peau vers la lingotière contrôle l'intensité de la contraction de la peau, son déplacement et son retrait des parois de la lingotière. Les modifications qui en résultent en ce qui concerne la dimension de l'espace interfacial jouent un rôle important sur le transfert thermique. Nous avons utilisé conjointement la méthode aux éléments finis et la méthode aux différences finies pour résoudre ce comportement thermique et mécanique.

Pour étalonner le modèle, des données expérimentales provenant de coulées de l'aciérie d'Ilva-Dalmine ont été obtenues avec une lingotière d'un diamètre de 280 mm équipée de thermocouples et ayant une conicité linéaire de 1,8 %/m. Outre les températures moyennes mesurées par thermocouples à divers endroits, ont été également relevées les données importantes suivantes : la vitesse de coulée moyenne, l'augmentation moyenne de température de l'eau de refroidissement, les paramètres de l'oscillation de la lingotière, la composition de l'acier et les caractéristiques de la poudre de lubrification.

Après étalonnage du modèle, une étude paramétrique a été entreprise pour estimer la conicité idéale des parois de la lingotière ainsi que le transfert thermique, le comportement de la poudre et les autres paramètres attendus dans ces conditions idéales. Finalement, nous avons examiné l'influence de nombreux paramètres de coulée dont la vitesse de coulée, le type de poudre, la nuance d'acier et les dimensions de blooms.

Cette analyse mathématique du transfert de chaleur, du comportement du flux dans la lingotière, de la contraction et de la distorsion de l'acier en lingotière pour la coulée continue de blooms d'acier a donné des idées pour l'optimisation de la conicité de la lingotière. La peau de l'acier tend à se contracter davantage dans la partie supérieure de la lingotière où la conicité devrait être forte. Plus bas, la résistance thermique d'une peau plus épaisse qui peut se combiner avec une couche plus épaisse de poudre de lingotière réduit l'extraction du flux de chaleur. Cela ralentit la vitesse de diminution de la température de peau, ce qui produit moins de contraction de peau et ainsi la conicité pourrait être faible.

Par conséquent, une lingotière avec une seule pente linéaire n'est jamais la meilleure pour couler des blooms ronds. Dans cette étude, pour s'adapter à la courbure continue de la peau en traction, on a choisi une conicité en trois parties linéaires précisée ci-après :

– zone du haut (du ménisque à 80 mm) : 4,5 %/m ;

– milieu (80 à 300 mm) : 1,0 %/m ;

– en bas (300 mm à sortie de lingotière) : 0,6 %/m.

Ces valeurs se rapportent à la pente des parois de lingotière à la température ambiante avant les déformations élastiques calculées pendant l'opération. Cette conicité a été calculée pour s'adapter à la contraction à une vitesse de coulée de 0,5 m/min. Cependant, c'est une conicité raisonnable pour des vitesses plus importantes où l'on est prudent en ce qui concerne le collage de la veine dans la lingotière.

Les calculs du modèle indiquent que la conicité idéale dépend étroitement des propriétés de la poudre, car elle détermine le flux dans l'interface en termes de conductibilité thermique, de viscosité et des taux de consommation. Le taux de consommation dépend de phénomènes complexes tels que l'usage de l'oscillation, le comportement fluodynamique et thermique de la surface du ménisque, que l'on n'a pas pris en considération dans ce modèle. La conicité idéale pourrait changer avec le type de poudre et son taux de consommation qui pourraient être mis sous contrôle.

La teneur en carbone dans la plage critique de 0,1 % est associée avec un flux de chaleur réduit et une dilatation thermique plus forte. Ces deux effets de la contraction de la peau de l'acier tendent à se compenser ; c'est pourquoi la conicité idéale n'est pas sensiblement affectée.

Finalement, le changement de format du bloom pourrait n'avoir aucun effet sur le pourcentage de conicité idéale.

These phenomena are intimately coupled, because the amount of the heat transferred from the shell to the mold controls the extent of the shell shrinkage and its movement away from the mold walls. The consequent changes in the gap size strongly affects the heat transfer. Coupled finite-element and finite difference methods have been used to solve for this thermal and mechanical behaviour.

To calibrate the model, experimental data from the heats cast at Ilva-Dalmine steel works were obtained by means of a thermocouple equipped mold with a nominal diameter of 280 mm and a 1.8%/m linear taper. In addition to the average temperatures at specified locations measured by thermocouples, the following crucial data were also recorded: the average casting speed, the average temperature increase of the cooling water, the mold oscillation parameters, steel composition and the properties of the lubricating powder flux.

Having calibrated the model, a parametric study was performed to predict the ideal taper of the mold walls and the associated heat transfer, powder behaviour, and other parameters expected under these ideal conditions. Finally, the influence of important casting variables on ideal taper were examined, including casting speed, powder type, steel grade and bloom dimensions.

■ HEAT CONDUCTION IN THE MOLD

Temperature in the mold is determined with a steady-state, two-dimensional calculation in the upper part of the mold, where the heat flow is highly non-linear and a one-dimensional calculation in the lower portion.

The boundary condition on the internal surface is the heat flux crossing the interfacial gap. Heat convection with the mold cooling water is applied as the external boundary condition.

A typical example of the calculated temperature contours in the mold is given in *figure 2*. The location of the maximum temperature is always found below the meniscus because two-dimensional heat transfer through the mold due to cooling above the meniscus extracts heat from the meniscus region.

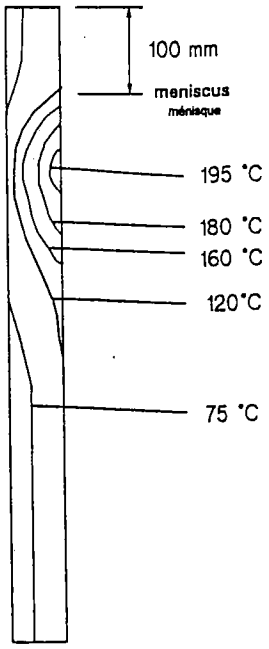

Fig. 2 – Temperature contours through the mold thickness.

Fig. 2 – Isothermes à travers l'épaisseur de la lingotière.

■ HEAT TRANSFER ACROSS THE INTERFACIAL GAP

Heat flux extraction from the steel is governed primarily by heat conduction across the gap, whose thermal resistance is determined by the thermal properties and thicknesses of the solid and liquid powder layers, which are incorporated into a single equivalent air gap. Nonuniformities in the flatness of the shell surface, represented by the oscillation marks, have an important effect on the local thermal resistance and are incorporated into the model as an effective average depth of the marks, d_0.

The model for gap heat conduction is illustrated in *figure 3* where the resistance model is shown as well and is given by the following equation :

$$q = \frac{T_s - T_m}{\frac{d_a}{k_a} + \frac{d_s}{k_s} + \frac{d_l}{k_l} + \frac{d_0}{k_0}} + \frac{m^2 \sigma (T_s^4 - T_m^4)}{0.75\, a\, (d_l + d_s) + \frac{1}{\varepsilon_s} + \frac{1}{\varepsilon_m} - 1} \qquad [1]$$

where

q = heat flux transferred across gap,

T_s = surface temperature of the steel shell,

T_m = temperature of the copper mold,

d_a = total effective air gap thickness,

d_s = local solid flux layer thickness,

d_l = local liquid flux layer thickness,

d_0 = effective thickness of the oscillation marks,

k_a = thermal conductivity of air,

k_s = thermal conductivity of solid flux,

k_l = thermal conductivity of liquid flux,

k_0 = effective thermal conductivity of material in oscillation marks,

a = absorption coefficient,

m = refraction index,

σ = Stefan - Boltzmann constant,

ε_s = emissivity of steel

ε_m = emissivity of copper mold

■ MOMENTUM BALANCE ON THE FLUX LAYER

Flux is assumed to flow down the gap as two distinct layers : solid and liquid. The solid layer is assumed to move at a constant velocity, V_s, which is always greater than zero and less than casting speed.

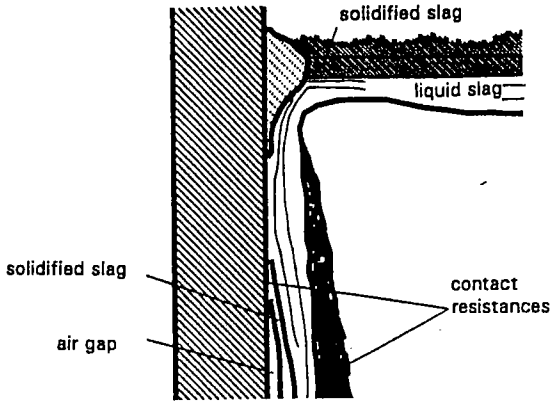

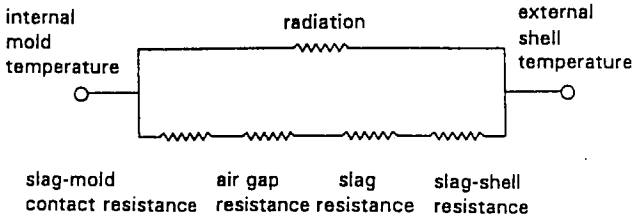

Fig. 3 – Model for gap heat conduction between the shell and the mold.

Fig. 3 – Modèle de conductivité de chaleur entre la peau de l'acier et la lingotière.

$$V_s = f_c V_c \qquad 0 < f_c < 1 \qquad [2]$$

The casting speed is imposed at the point of contact between the shell and the liquid layer, which is assumed to flow in a laminar manner, owing to its high viscosity. Flow in the liquid layer is given by the Navier-Stokes equation, where τ_{yz} is the tangential shear stress:

$$\frac{\partial \tau_{yz}}{\partial_y} = -\rho g \qquad [3]$$

where :

z = casting direction,

y = radial direction,

r = average density of flux,

g = gravity acceleration.

The tangential shear stress, τ_{yz}, is related to the viscosity of the molten flux, μ, by :

$$\tau_{yz} = \mu \frac{\partial v_z}{\partial_y} \qquad [4]$$

and the viscosity, μ, is assumed to vary exponentially with distance across the gap, according to the temperature:

$$\mu = \mu_0 \left(\frac{T_0 - T_{sol}}{T - T_{sol}} \right)^n \qquad [5]$$

The previous approximated equation form has been chosen instead of the more usual : $\mu = \mu_s e^{-AE/RT}$ because it is easiest to use in the calculations.

T_{sol} is the solidification temperature of the flux, μ_0 is the viscosity measured at T_0, and n is an empirical constant chosen to fit all of the measured data. Solving equations [2 to 5] yields the velocity distribution across the flux layers. Integrating across the liquid region yields an average velocity for the liquid layer, V_l :

$$V_l = \frac{v_c + v_s (n+1)}{(n+2)} + \frac{\rho g d_l^2}{\mu_0 (n+2)^2 (n+3)} \qquad [6]$$

The effect of gravity represented in the second term is small, owing to the thin gap sizes typically found.

■ MASS BALANCE ON THE FLUX LAYER

A third balance equation was imposed to express the fact that the known powder consumption must equal the total powder flow rate past every location down the interfacial gap. The following equation expresses this condition as balance on the total volumetric flux flow rate per unit width in x direction, Q ($m^2 s^{-1}$) as the density was assumed to be constant:

$$Q = V_s d_s + V_l d_l + V_c d_e \qquad [7]$$

In this time-averaged model, the effects of oscillation are incorporated directly only through the influence of the width, depth and pitch of the oscillation marks on the effective thicknesses contributing to consumption, d_e, and heat transfer, d_0.

The total thickness of the flux layers is related to shell shrinkage (d_{Fe}), the mold distorsion, the mold taper and the possible presence of an air gap, which together determine the size of the interfacial gap :

$$d_a + d_s + d_l + d_e = d_{Fe} - d_m \qquad [8]$$

Equations [2 to 8] together provide a relationship between the total flux thickness and the velocity of the solid flux at every distance down the gap. With simultaneous solution of equation [1], heat transfer across the mold/shell gap can be solved.

Two different regions can be distinguished down the mold, according to the lubrication condition. Close to the meniscus, the first region includes a liquid flux layer, which exists where the gap temperature exceeds the given mold flux solidification temperature. Flux in the oscillation marks remains liquid longer, due to the higher local temperature there. As the shell surface temperature decreases, the flux entrapped in the oscillation marks cools and solidifies once the local shell temperature falls below the flux solidification temperature.

The second region considers totally solid flux, which travels at a uniform speed across the gap.

The steel shell is assumed to be stronger than the flux layer, once it has travelled a short distance below the meniscus. Thus the mold flux must accomodate the interfacial gap imposed by the shrinking shell and position of the mold wall. If the gap increases, the powder either slows down, on average, or an air gap must form. If the gap decreases, the speed of the powder must increase. Increasing the average speed of powder which has completely solidified has the physical consequence of tearing it.

■ HEAT CONDUCTION IN THE SOLIDIFYING STEEL SHELL

A finite-difference model is used to calculate temperature in the solidifying shell as it moves down through the mold, by solving the following transient, one-dimensional heat conduction equation :

$$\frac{\partial}{\partial x} k \frac{\partial T}{\partial x} = \rho C_p \frac{\partial T}{\partial t} \qquad [9]$$

where:

x is the abscissa along the shell thickness, T is the local temperature, ρC_p is the steel heat capacity.

Latent heat is incorporated into the specific heat. The imposed boundary conditions are given by q on the external surface against the interfacial gap, defined in Eq. [1] and on the internal solid/liquid steel interface, a «superheat flux» function is imposed.

Steel is poured into the mold at a temperature of about 30 °C above the liquidus temperature. Before it solidifies, it must first cool to the liquidus temperature. Due to turbulent convection in the liquid pool, the superheat contained in this liquid is not distributed uniformly. A fluid flow model is used to determine the heat flux delivered to the

solid-liquid interface due to the superheat dissipation. The initial condition on the liquid steel at the meniscus is then simply the liquidus temperature.

For the specific round bloom caster considered, the single port of the submerged entry nozzle points straight downwards. Jet dynamics studies (1) have shown that a jet expanding into a larger concentric pipe will spread as it entrains fluid to first impinge upon the outer walls at a distance from the inlet of about 9 times the pipe radius. Thus, the maximum heat delivered to the dendritic interface of the solidifying steel occurs at this distance below the meniscus.

■ THERMO-MECHANICAL ANALYSIS OF THE SOLIDIFYING STEEL SHELL

Coupled thermal stress calculations have been performed on the solidifying steel using the finite element program, Concast (2). A two-dimensional mesh of one quarter of a section through the circular mold normal to the mold axis has been analyzed. The model simulates the behaviour of a slice that begins at the meniscus and travels down through the mold. At each position down the mold, two separate calculations are performed, alternating between the thermal and stress analysis phases. Calculations are based on the heat flux applied to the shell exterior found at the previous step.

Loads arise solely due to the non-linear temperature gradients found in the steel shell. The effects of hydrostatic pressure from the liquid steel have been neglected, because bulging of the shell is small in the small rounds under consideration. Moreover, the present study is concerned primarily with ideal casting conditions. With a proper mold taper, the constraining mold walls should balance the ferrostatic load and avoid bulging.

The stress calculation was performed to determine the shrinkage profile of the shell down the mold, needed for calculating the ideal mold taper, in addition to serving as input for the equations involving the interfacial gap size. This calculation decomposes the total strain into the sum of three components : the thermal contraction, the plastic strain and the elastic strain. The first of these has been found to dominate. It has been seen that the thermal strain at the surface of the shell matches quite closely with the average total strain across the thickness of the shell, which controls its shrinkage. This is because this outer layer of steel solidifies first and shrinks relatively stress free, while the later, inner steel to solidify against it is weaker and accomodating. Thus, the entire, complex mechanical behaviour of the shell can be approximated quite reasonably by the following simple calculation for the shrinkage of the shell, d_{Fc} :

$$dFc = \frac{TLE(T_{sol}) - TLE(T_{Fc})}{L}$$

where

TLE = thermal linear expansion function for the given steel,

T_{sol} = solidus temperature,

L = effective mold length.

■ MOLD DISTORTION

The final phenomenon determining the size of the interfacial gap is thermal distortion of the mold. The results of elastic thermal-stress calculations revealed that the mold acts as a relatively-unconstrained, thin-walled tube, which expands outward in proportion to its temperature. Thus, the mold distortion, d_m is then reasonably approximated by the simple equation:

$$d_m = (\alpha T_{init} - \alpha T'_m + tap)\, R$$

where

α = copper linear thermal expansion coefficient (17.7×10^{-6} per °C)

T_{init} = initial temperature of mold (30 °C)

tap = mold taper

Here, the integrated average temperature through the mold wall, T'_m, is used to calculate the distorted position of the mold wall as a function of distance down the mold. Assuming the mold behaves elastically, this calculated shape should arise during operation for every heat, and return to zero distorsion after cooling to ambient temperature. The residual deformation due to plastic distortion which can accumulate over many heating cycles to elevated temperature was neglected.

■ SOLUTION PROCEDURE

The model requires simultaneous solution of three different systems of equations: 1-D transient heat conduction and solidification of the steel shell, 2-D steady state heat conduction in the mold and the equations for the mold flux momentum and mass balances, the mold distorsion and the steel shell shrinkage.

Briefly, the calculations proceed as follows:

A 1-D finite difference calculation is first performed within the steel shell, interface, and mold, to provide a reasonable initial guess. This calculation begins at the meniscus and proceeds down the mold with time according to the given casting speed. At each time step, or distance down the mold, iteration is performed after initially assuming the conditions from the previous step.

Based on the calculated heat flux profile down the interfacial gap, the mold temperatures in the upper portion of the mold are recalculated using the two-dimensional model. Next, the equations to calculate the mold distortion, shell shrinkage, flux layer thicknesses and the temperature distribution in the gap and shell are resolved, starting over again at the meniscus.

The entire procedure is repeated until convergence is achieved, which generally requires 3 - 4 iterations through the model. The result is a self consistent prediction of mold heat transfer (including temperature and heat flux within the shell, interface and mold) and the deformation profile down the mold (including the shell shrinkage, flux layer thicknesses and velocities, mold distortion).

■ MODEL CALIBRATION

In order to calibrate the model, simulations were performed to match the casting conditions of two different heats, 403 and 422, which were cast on Ilva-Dalmine round bloom caster in a mold where thermocouple temperatures and other measurements were available. The casting conditions are given in *table I*.

The model was run many times through trial and error to find values of the model parameters that allowed all of the mold temperatures and the cooling water temperature rise predicted by the model to simultaneously match the measurements. Specifically, adjustments were made to the water-side heat transfer coefficient, within strict limits, the velocity of the solid flux layer at the meniscus and the value

Table I : Casting conditions.

Tableau I : Conditions de coulée.

	Heat 403	Heat 422
Casting speed (m/min)	0.88	0.66
Steel grade C	0.20	0.28
Mn	1.45	0.70
S	0.03	0.01
P	0.03	0.18
Si	0.43	0.18
Cr	0.25	1.10
Ni	0.25	0
Cu	0.25	0
Mo	0.10	0.36
Al	0.03	0.30
Flux solidification temperature (°C)	1 210	1 235
Flux conductivity (W/m.°C)	1	2
Flux viscosity at 1 300 °C (Pa.s)	11.7	5.5
Flux density (kg/m^3)	2500	2500
Powder consumption (kg/m^2)	0.5635	0.4606
Oscillation mark depth (mm)	0.375	0.405
Oscillation mark width (mm)	4	4
Oscillation frequency (hertz)	0.026	0.77
Stroke (mm)	10	10
Mold copper thickness (mm)	21	21
Distance of meniscus from top of mold (mm)	100	100
Cooling water temperature (°C)	30	30
Cooling water pressure (MPa)	0.606	0.606
Cooling water velocity (m/s)	4.328	4.328
Air gap thickness (mm)	Z gap 0. 0. 20 0.025 60 0.01 400 0.03 600 0.03	Z gap. 0. 0. 20 0.105 60 0.07 400 0.052 600 0.048

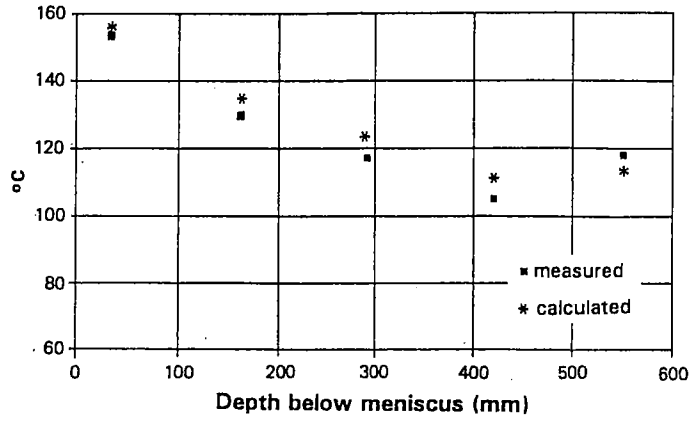

Fig. 4 – Comparison between measured and calculated temperatures for heat 403.

Fig. 4 – Comparaison entre les températures mesurées et calculées pour la coulée 403.

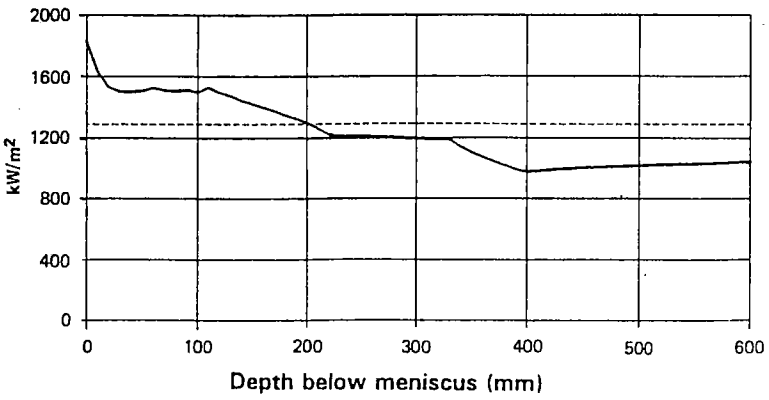

Fig. 5 – Heat flux curve for heat 403. The dotted line represents the mean value given by experimental data.

Fig. 5 – Courbe du flux de chaleur pour la coulée 403. La ligne pointillée représente la valeur moyenne fournie par les données expérimentales.

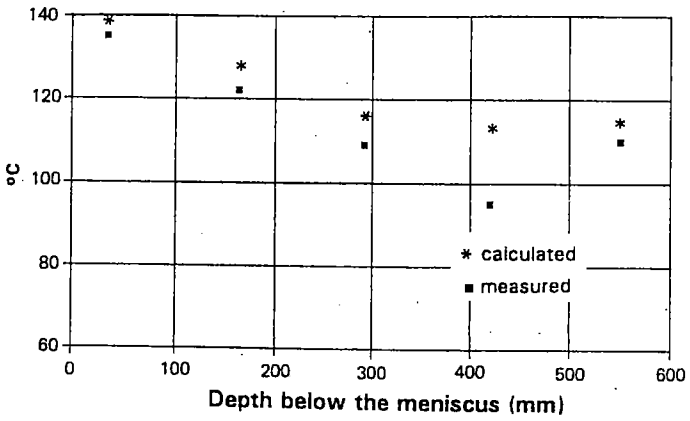

Fig. 6 – Comparison between measured and calculated temperatures for heat 422.

Fig. 6 – Comparaison entre les températures mesurées et calculées pour la coulée 422.

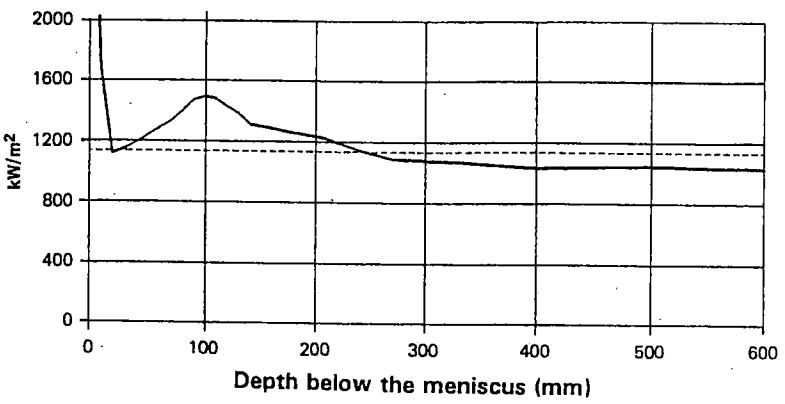

Fig. 7 – Heat flux curve for heat 422. The dotted line represents the mean value given by experimental data.

Fig. 7 – Courbe du flux de chaleur pour la coulée 422. La ligne pointillée représente la valeur moyenne fournie par les données expérimentales.

of the contact resistances down the mold. All the parameters were either fixed as input conditions, such as the powder consumption rate and oscillation mark width and depth, or calculated by the model, such as temperatures, powder layer thicknesses and solid flux velocity ratio.

Sample comparison between the calculated and measured mold temperatures and the corresponding heat flux profiles are given in *figures 4 to 7* for the two test cases. In the *figures 8 and 9* are represented the corresponding calculated deformed shapes of the shell and mold. Mold distorsion is seen to be a relatively minor consideration.

The distance between the distorted mold and shell positions is equal to the gap size. In the *figures 8 and 9*, the gap thickness is seen to decrease from top to bottom of the mold. This has the consequence of increasing the speed of the powder. However, this result suggests compression and break-up of the powder would occur under these conditions.

These results also indicate that the shell attempts to shrink away from the upper portion of the mold, while it is pushed against the lower portion of the mold. To match this shrinkage, it is clear that taper should be increased high in the mold and decreased lower down.

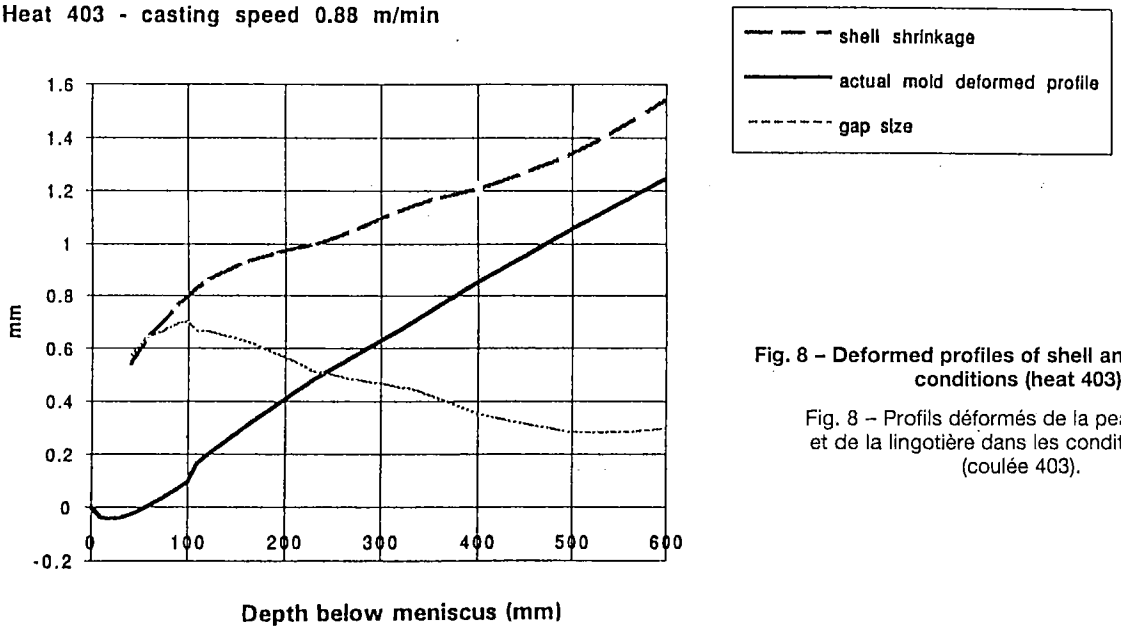

Fig. 8 – Deformed profiles of shell and mold in actual conditions (heat 403).

Fig. 8 – Profils déformés de la peau de l'acier et de la lingotière dans les conditions réelles (coulée 403).

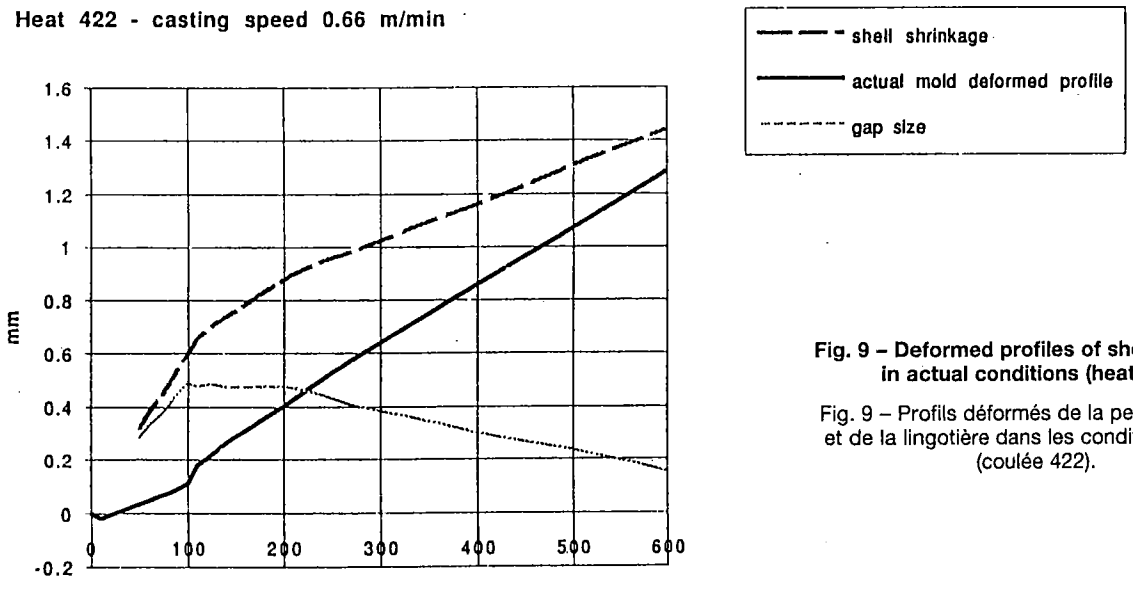

Fig. 9 – Deformed profiles of shell and mold in actual conditions (heat 422).

Fig. 9 – Profils déformés de la peau de l'acier et de la lingotière dans les conditions réelles (coulée 422).

■ TAPER OPTIMIZATION

The model was next applied to predict the consequences of using a different taper, in order to achieve better casting performance. In performing these ideal taper calculations, three separate criteria were satisfied : no air gap, no shell compression, uniform gap thickness.

Too small a taper cause an air gap to form, as the flux is unable to completely fill the large gap that tends to form between the shell and the mold. Too high a taper causes the predicted speed of the mold flux to exceed the casting speed, which might indicate an unreasonable degree of compression by the mold against the shell. Finally, the velocity and the total thickness of the powder layers were sought to remain as constant as possible down the mold. This is believed to minimize the chances of cracking the powder layer, which is likely when there is acceleration or deceleration of the brittle solid flux layer.

For the two test heats used in calibrating the model, ideal taper satisfying all three criteria was achieved by means of three-fold tapers. The *figures 10 and 11* show the corresponding calculated deformed shell and mold profiles.

The model was next used to investigate the effects of casting parameters on the ideal taper calculation. These important variables included : casting speed, powder type, steel grade and bloom size.

■ CASTING SPEED

The effect of increasing the casting speed on the ideal taper was investigated for the conditions of test case 403, including the corresponding measured decrease in mold flux consumption. The results are listed in *table II* and presented in *figure 12*.

Increasing casting speed tends to decrease the ideal taper, owing to the hotter shell and corresponding smaller amount of shrinkage found when there is less time in the mold. However, the increase in casting speed and decrease in ave-

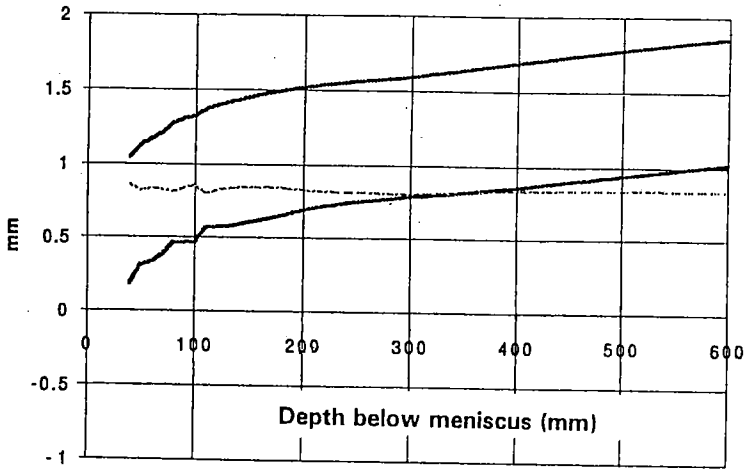

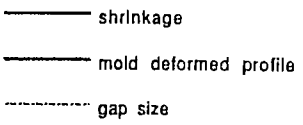

Fig. 10 – Ideal taper for casting speed 0.88 m/min, same casting conditions as 403 heat.

Fig. 10 – Conicité idéale pour une vitesse de coulée de 0,88 m/min. Mêmes conditions de coulée que pour l'essai 403.

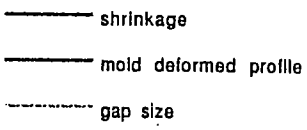

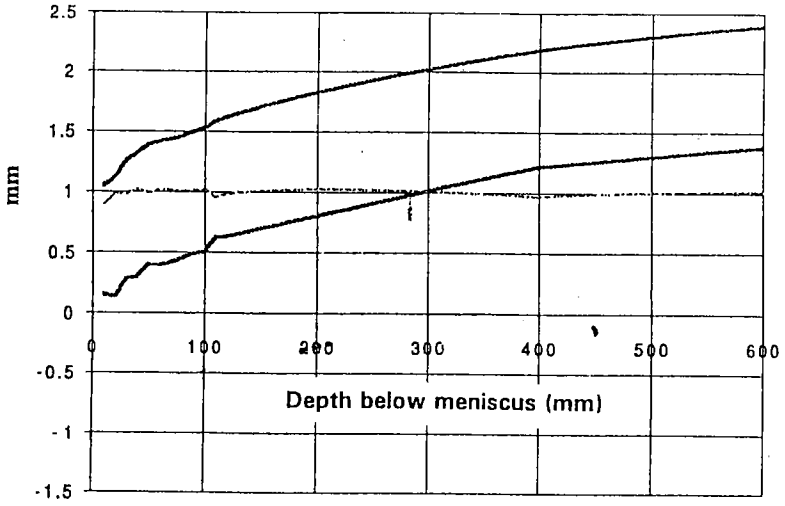

Fig. 11 – Ideal taper for casting speed 0.66 m/min, same casting conditions as 422 heat.

Fig. 11 – Conicité idéale pour une vitesse de coulée de 0,66 m/min. Mêmes conditions de coulée que pour l'essai 422.

tion, the deeper oscillation marks produce a greater average resistance to heat transfer, including a thicker average flux layer. This tends to increase the steel shell temperature and reduce the amount of shrinkage.

These two phenomena tend to compensate for each other. However, this gap becomes filled with a thicker powder layer. The result is a similar ideal taper, although the heat flux and solidified shell thickness are smaller for the lower carbon steel.

■ BLOOM SIZE

A comparative calculation on the effect of bloom size was conducted for the 403 heat, by increasing the mold diameter from 280 to 360 mm. With other parameters remaining constant, the increased diameter produces a proportional increase in the distortion and shrinkage. However, the ideal taper, expressed in %/m is always predicted to remain the same for any bloom size.

■ CONCLUSIONS

The present mathematical analysis of heat transfer, mold flux behaviour, steel shrinkage and distortion in the mold of a continuous steel bloom caster has revealed insights into the optimization of mold taper.

The steel shell tends to shrink most in the upper regions of the mold, where taper should be high. Lower down, the thermal resistance of the thicker steel shell, possibly combined with a thicker mold powder layer, lowers the heat flux extracted. This lowers the rate of decrease of the shell temperature, which produces less shrinkage so taper should be small.

Thus, a single linearly sloped mold is never optimal when casting round blooms. In the present work, the following three-fold linear taper was chosen to approximately match the continuous curvature of the shrinking steel shell :

- upper region (meniscus - 80 mm).....4.5 % / m
- middle region (80 - 300 mm).....1.0 % / m
- lower region (300 mm - mold exit) .....0.6 % / m

These values refer to the ambient temperature slope of the mold walls, prior to the elastic distortion calculated during operation. This taper was calculated to match shrinkage at a casting speed of 0.5 m/min. However, it is a reasonable taper for higher speeds also, where it is conservative regarding sticking of the strand in the mold.

The model calculations indicate that ideal taper in general is critically dependent on the powder properties as these govern heat flux across the interface in terms of thermal conductivity, viscosity and consumption rates. The consumption rate depends upon complex phenomena such as oscillation practice, fluid-dynamic and thermal behaviour of the meniscus surface, which are not considered in the present model. Ideal taper should be changed with powder type and its rate of consumption, which should be monitored.

Carbon content in the critical 0.1% range is associated with reduced heat flux and higher thermal expansion. These two effects of shrinkage of the steel shell tend to compensate, so the ideal taper is not significantly affected.

Finally, changing bloom size should have no effect on ideal percent taper.

■ REFERENCES

(1) KHODADADI (J.M.) et al. Experimental and numerical study of confined coaxial turbulent jets. *AIAA Journal*, vol. 27, n° 5 (June 1987), p. 532-541.

(2) MOITRA (A.) et al. Thermo-mechanical model of steel shell behaviour in the continuous casting mold. TMS Annual Meeting, San Diego (March 1991).

(3) IIDA (T.) et al. Equation for thermal conductivity of molten salts and slags. Private communication.